Nonadiabatic molecular dynamics with subsystem density functional theory: application to crystalline pentacene

OPEN ACCESS
IOP Publishing
Journal of Physics: Condensed Matter
J. Phys.: Condens. Matter **36** (2024) 385901 (17pp)
https://doi.org/10.1088/1361-648X/ad577d

Nonadiabatic molecular dynamics with subsystem density functional theory: application to crystalline pentacene

Qingxin Zhang[1], Xuecheng Shao[2], Wei Li[3], Wenhui Mi[4,5], Michele Pavanello[2] and Alexey V Akimov[1,*]

[1] Department of Chemistry, University at Buffalo, The State University of New York, Buffalo, NY 14260, United States of America
[2] Department of Physics, Rutgers University, The State University of New Jersey, Newark, NJ 07102, United States of America
[3] School of Chemistry and Materials Science, Hunan Agricultural University, Changsha 410128, People's Republic of China
[4] Key Laboratory of Material Simulation Methods & Software of Ministry of Education, College of Physics, Jilin University, Changchun 130012, People's Republic of China
[5] State Key Laboratory of Superhard Materials, Jilin University, Changchun 130012, People's Republic of China

E-mail: alexeyak@buffalo.edu

Received 24 April 2024, revised 31 May 2024
Accepted for publication 12 June 2024
Published 21 June 2024

Abstract

In this work, we report the development and assessment of the nonadiabatic molecular dynamics approach with the electronic structure calculations based on the linearly scaling subsystem density functional method. The approach is implemented in an open-source embedded Quantum Espresso/Libra software specially designed for nonadiabatic dynamics simulations in extended systems. As proof of the applicability of this method to large condensed-matter systems, we examine the dynamics of nonradiative relaxation of excess excitation energy in pentacene crystals with the simulation supercells containing more than 600 atoms. We find that increased structural disorder observed in larger supercell models induces larger nonadiabatic couplings of electronic states and accelerates the relaxation dynamics of excited states. We conduct a comparative analysis of several quantum-classical trajectory surface hopping schemes, including two new methods proposed in this work (revised decoherence-induced surface hopping and instantaneous decoherence at frustrated hops). Most of the tested schemes suggest fast energy relaxation occurring with the timescales in the 0.7–2.0 ps range, but they significantly overestimate the ground state recovery rates. Only the modified simplified decay of mixing approach yields a notably slower relaxation timescales of 8–14 ps, with a significantly inhibited ground state recovery.

Keywords: nonadiabatic molecular dynamics, subsystem density functional theory, frozen density embedding, trajectory surface hopping, excitation energy relaxation, pentacene

* Author to whom any correspondence should be addressed.

1. Introduction

Quantum processes play a critical role in many natural systems such as light-harvesting and photosynthetic complexes [1–4], biological vision [5, 6] and light sensing [7–10] systems as well as in artificial photocatalytic [11–14] and photovoltaic [15–17] materials, materials for quantum sensing applications [18–20], or qubits [21–23], to name a few. Quantum coherence facilitates efficient and directional excitation energy transfer in the light-harvesting complexes [24–26], coupled electron-proton transfer [27–29], quantum tunneling [30–32], is critical to biological systems [33], and nonradiative energy relaxation, which realizes mechanisms of protection from the photodamage [34–38]. Exciton and multiple exciton generation [39, 40], singlet fission [41–47], triplet energy transfer and sensitization [48–50], charge transfer [51–53] and charge carrier trapping [54, 55] are examples of processes that determine the operation of artificial energy-harvesting and conversion materials. Photoinduced nuclear rearrangements constitute the basis of artificial photocatalysis [56–59] and are foundational to the functioning of biological photoreceptors [60–62].

In most of the above examples, quantum transitions between electronic states mediated by the electron-vibrational (or electron–phonon) nonadiabatic (NA) couplings are of interest. Modeling the dynamics of multiple electronic or excitonic states whose evolution is affected by their coupling to nuclear vibrations can be conducted within the framework of nonadiabatic quantum dynamics, often referred to as nonadiabatic molecular dynamics (NA-MD). To date, multiple NA-MD methods have been developed, ranging from the mixed quantum-classical (MQC) methods such as Ehrenfest [63, 64] and trajectory surface hopping (TSH) [65–68] techniques to semiclassical wave packet propagation and fully quantal [69] methods. Due to their simplicity, low computational cost, and reasonable accuracy, the approximate MQC techniques have found their wide use in modeling NA dynamics in many condensed-matter [70–85] and molecular systems [86–89]. However, such modeling in extended systems is often hindered by two factors: the intrinsic complexity of quantum dynamics itself and the steeply scaling costs of reliable electronic structure calculations. The first limitation is addressed by adopting the MQC strategies that approximate fully quantum dynamics via coupled or independent trajectories although at the price of the need for an accurate sampling of possible outcomes of the coupled electron-nuclear dynamics with such trajectories. Fortunately, in many extended systems the neglect of back-reaction approximation (NBRA) of Prezhdo and co-workers [90, 91] can be adopted. It allows for significantly reducing the costs of the TSH computations by disregarding multiple possible nuclear histories in lieu of a single guiding trajectory that parameterizes the evolution of electronic degrees of freedom, including possible state transitions and coherence decay dynamics. A number of works also addressed other complexity issues relevant to quantum dynamics in extended systems such as using larger integration timesteps [92, 93], avoiding the use of ill-behaved nonadiabatic couplings (NACs) [94–96], or relying on effieint tracking of the state identities in dense manifolds of states [97–99], a common situation in large-scale systems.

The second limitation of the NA-MD methods when applied to modeling large atomistic systems is the expense of the underlying electronic structure calculations. To address this kind of limitations, a number of approaches have been devised. They include using semiempirical methods such as extended Hückel theory [100–103], intermediate neglect of differential overlap [104], modified neglect of diatomic overlaps [94, 105, 106], collective electron oscillator [107–109], Austin Model 1 [110], and well as their combinations with classical force fields [111, 112]. Several groups have conducted NA-MD simulations using density functional tight-binding [113–116] as well as the extended tight-binding method [117–119]. More recently, the approaches based on using machine learning potentials or Hamiltonians started emerging as viable and practical routes to accelerating such kinds of calculations [120–124]. Besides using more efficient Hamiltonians, a number of works relied on reduced-scaling approaches which are particularly appealing for handling large-scale systems. For instance, Uratani and Nakai [125] incorporated the divide-and-conquer (DC) strategy to conduct Ehrenfest dynamics in giant fullerenes, Wang *et al* [126] developed a similar-in-spirit linearly scaling three-dimensional fragment scheme to conduct Ehrenfest dynamics simulations in large supercells of metal-organic perovskite solids. The Blumberger group developed the fragment orbital-based surface hopping [17] approach for modeling NA-MD and charge carrier transport in large supercells of organic crystals. Akimov [100] developed a TSH approach based on non-self-consistent fragment molecular orbitals and demonstrated its utility in modeling interfacial charge transfer dynamics with models involving several hundreds of atoms. More recently, yet another fragmentation-based TSH approach was reported by Wang *et al* [127] who used it in simulations of charge transport dynamics in large systems.

In this work, we explore yet another possibility of using the reduced-scaling electronic structure methods, namely the subsystem DFT (sDFT) [128], for modeling NA-MD in extended periodic systems. We rely on the sDFT implementation [129–132] within the embedded Quantum Espresso (eQE) package [128]. Recently, sDFT has been successfully employed for studying a range of phenomena and time/length scales, such as the structure of molecular liquids [133, 134], solvation [135, 136], spin systems [137], large biosystems [138–140] and an array of phenomena involving excited electronic states [141, 142]. For a more extensive overview of the prospects of using sDFT in various kinds of applications, we refer the reader to the excellent reviews on the topic by Jacob and Neugebauer [129, 132]. Despite the wide use of sDFT in more traditional electronic structure calculations, including in excited states calculations [140, 143, 144], sDFT is yet to unleash its full potential in the NA-MD simulations. To date, relatively few

NA-MD studies with sDFT have been reported, notably by the Luber group (via delta-SCF) [145, 146].

To enable such applications, we develop a new computational workflow for NA-MD calculations by interfacing the sDFT-based electronic structure calculations as done in the eQE package with the NA-MD calculations executed by the Libra software [147]. The developed methodology is demonstrated and assessed by applying it to modeling hot electron relaxation dynamics in organic crystals of pentacene, a promising material for organic solar cell applications. Pentacene has gained a lot of attention due to its potential to participate in multiple exciton generation and singlet fission [41, 91, 148–150] as well as being a popular acceptor in polymer-based heterojunction solar cells [45, 151–154]. The excited-state dynamics in pentacene have been extensively studied both experimentally [155–158] and computationally [41, 91, 159–161] due to its potential to surpass the Shockley-Queisser [43, 162] limit of solar energy conversion efficiency.

In the present form, our approach disregards the possibility of NA transitions between states belonging to different fragments. Thus, one must have a well-defined central system in which the NA transitions are to be studied. At the same time, the current sDFT approach enables self-consistent calculations of orbitals of different subsystems. In this regard, the fragmentation (subsystem) approach considered here is meant to accelerate the calculations of the system-environment interactions by partitioning the environmental sub-system. In this regard, the present approach is meant to describe the polarization and exchange effects of the environment on the NA dynamics of a central system of interest. We assume that the charge or excitation energy transfer effects between the central system and the environment can be neglected.

2. Theory and computational methodology

2.1. sDFT

The main concept underpinning sDFT is the realization that any electron density, $\rho(r)$, can be decomposed formally into a sum of subsystem electron densities, $\{\rho_I\}$:

$$\rho(r) = \sum_I \rho_I(r). \tag{1}$$

While the decomposition above is arbitrary, it can be put on formal grounds by requiring that each of the subsystem electron densities be determined variationally. That is, indicated by $E[\rho]$ the total energy functional, we impose:

$$\frac{\delta E}{\delta \rho_I(r)} = 0, \forall I. \tag{2}$$

Doing so leads to the following Kohn–Sham (KS) equation with constrained electron density, which needs to be simultaneously solved for each subsystem by the following KSCED:

$$\left[-\frac{1}{2}\nabla^2 + v_s[\rho_I](r) + v^I_{\text{emb}}[\{\rho_I\}](r)\right]\phi^I_i(r) = \varepsilon^I_i\phi^I_i(r). \tag{3}$$

In the above equation, the embedding potential for subsystem I is formally the functional derivative of the non-additive energy functional which is defined as

$$v^I_{\text{emb}}[\{\rho_I\}](r) = \frac{\delta E^{\text{nad}}[\{\rho_I\}]}{\delta \rho_I(r)}, \tag{4}$$

where the non-additive functional takes the form

$$E^{\text{nad}}[\{\rho_I\}] = E[\rho] - \sum_I E[\rho_I]. \tag{5}$$

So far, we have only indicated the functional dependence on the electron densities, however, it is understood that the total energy functionals require specification of the electron-nuclear interaction when evaluated with non-self-consistent electron densities. Programs such as eQE and several others [140, 163–166] implement sDFT. Both eQE and CP2K implement a simultaneous solution of equation (3) whereby after each SCF cycle, the subsystem electron densities are broadcast to the other subsystems, and new embedding potentials are generated. This allows these codes to be particularly well suited for running ab initio molecular dynamics simulations. Such is the case in our work.

2.2. Nonadiabatic molecular dynamics

The nonadiabatic dynamics of vibrationally-induced electronic transitions is studied with several quantum-classical TSH methods. Namely, we consider the most basic Tully's fewest switches surface hopping (FSSH) method [65] and global flux surface hopping (GFSH) of Wang *et al* [92], as well as several approaches that introduce decoherence correction. The latter includes the instantaneous decoherence at attempted hops (ID-A) of Nelson *et al* [167], the modified [168] simplified decay of mixing (mSDM) originated by Granucchi *et al* [169], and the decoherence-induced surface hopping (DISH) of Jaeger *et al* [170], although revised in a spirit similar to one reported by the Zhao group [171] as detailed below. In addition, we introduce a slight modification of the ID-A algorithm, in which the wavefunction collapse occurs not at every hop attempt event but at every frustrated hop, dubbed the instantaneous decoherence at frustrated hops (ID-F).

All methods are formulated on the same ground of the Born–Huang expansion of the electronic wave function. Namely, this wavefunction is given by a time-dependent superposition of the dynamical basis states, $\{\Phi_i\}$, chosen in the present work as excited Slater determinants:

$$\Psi(\boldsymbol{r},t) = \sum_{I=0}^{N-1} c_I(t)\ \Phi_I(\boldsymbol{r};\boldsymbol{R}(t)). \tag{6}$$

Here, $\{c_I(t)\}$ are the time-dependent amplitudes corresponding to chosen adiabatic basis state functions, Φ_i. Following multiple prior studies [39, 91], the basis functions Φ_i are chosen as excited Slater determinants with various single excitations involving active occupied and unoccupied

orbitals. The latter are parametrically dependent on nuclear coordinates, $\boldsymbol{R}$, that is $\Phi_i = \Phi_I(\boldsymbol{r};\boldsymbol{R}(t))$. This dependence originates from the dependence of the corresponding electronic Hamiltonian, $\hat{H}_{el}(\boldsymbol{r};\boldsymbol{R}(t))$, on the nuclear trajectories:

$$\hat{H}_{el}(\boldsymbol{r};\boldsymbol{R}(t))\ \Phi_I(\boldsymbol{r};\boldsymbol{R}(t)) = E_i(R(t))\ \Phi_I(\boldsymbol{r};\boldsymbol{R}(t)). \quad (7)$$

In this work, we adopt the classical path approximation [65], which states that nuclei are treated classically using the forces of the active electronic state. Furthermore, we employ NBRA according to which the electronic excitations do not affect the motion of nuclei. In practice, the nuclear trajectories are precomputed using the ground state adiabatic MD coupled to a thermostat. The resulting nuclear trajectories, $\{\boldsymbol{R}(t)\}$, are termed the guiding trajectories and act as parameters that control the evolution of electronic wavefunction, equation (6). The electronic wavefunction evolves according to the time-dependent Schrodinger equation (TD-SE). Within the basis of NBRA-guided adiabatic electronic states, the TD-SE simplifies to:

$$i\hbar\frac{\partial c_i(t)}{\partial t} = \sum_j \left[E_j(t)\,\delta_{i,j} - i\hbar D_{i,j}(t)\right] c_j(t) = \sum_j H^{\text{vib}}_{i,j}(t)\,c_j(t). \quad (8)$$

Here, $E_j(t)$ is the adiabatic energy of the state j as determined from equation (7), $D_{i,j}(t) = \langle \Phi_i | \frac{\partial}{\partial t} \Phi_j \rangle$ is the NAC matrix element for the pair of states i and j, respectively, and $\delta_{i,j}$ is the Kronecker delta. The expressions $H^{\text{vib}}_{i,j}(t) = E_j(t)\,\delta_{i,j} - i\hbar D_{i,j}(t)$ can be regarded as matrix elements of the effective vibronic Hamiltonian. Although the TD-SE depends on the NACs, in practice we employ the local diabatization (LD) approach [94, 96, 172] to evolve the amplitudes. This algorithm helps enforce the correct state following, especially when trivial crossings are encountered. In addition, it also enforces the consistency of the electronic state phases along the guiding trajectories. The LD calculations require only the time-overlaps of basis states (Slater determinants), $O_{i,j}(t,t+\Delta t) = \langle \Phi_i(t) | \Phi_j(t+\Delta t) \rangle$. Such time-overlaps can be computed from the time-overlaps of the KS orbitals, $o_{ab}(t,t+\Delta t) = \langle \phi_a(t) | \phi_b(t+\Delta t) \rangle$ using the Lowdin formula [173], as detailed elsewhere [174].

An important aspect of computing time overlaps in plane-wave (PWs) codes like eQE is worth mentioning. Namely, the use of the pseudopotentials in such calculations, particularly ultrasoft pseudopotentials (USPP) [175], makes the corresponding KS orbitals non-orthogonal. Their orthogonality is only mediated by a metric, $\hat{S}$, which ensures $\langle \phi_i | \hat{S} | \phi_j \rangle = \delta_{ij}$. Because the metric is itself orbital-dependent, it is not possible to define one that formally connects orbitals at time t with orbitals at the time $t+dt$. We therefore approximate such metric with $\hat{S}(t+dt)$. This is a common approximation that is also invoked in real-time time-dependent density functional theory and Ehrenfest dynamics with USPPs [176–178]. Another complication worth mentioning is the notorious phase ambiguity/inconsistency problem [179, 180] of canonical orbitals. That is, if ϕ_i is a normalized eigenfunction of the KS Hamiltonian so is $e^{i\theta}\phi_i$. Since subsystems in sDFT are finite, we can impose without loss of generality the orbitals to be real. To handle the phase problem, we simply impose the elements of the overlap matrix to be positive, $O_{ij} \geqslant 0$. In this way, the sign is consistent throughout the simulation. While it is possible to have non-positive matrix elements, their occurrence is rare and unlikely given the small dt considered ($dt \approx 1$ fs). In addition, such time overlaps are used furtherr in the LD procedure, which also imposes the consistency of phases and characters of the evolved states.

Based on the evolved amplitudes of the adiabatic states, the state transitions are defined. In the FSSH algorithm of Tully [65], the state hops are attempted with the probabilities given by:

$$P^{\text{prop,FSSH}}_{i\to j}(t,t+\Delta t) = \max\left(0, \frac{\Delta t}{\hbar\rho_{ii}(t)} Im\left[\rho_{ij}H^{\text{vib}}_{ji} - H^{\text{vib}}_{ij}\rho_{ji}\right]\right). \quad (9a)$$

Here, $\rho_{ij} = c_i c_j^*$ is the coherence matrix element. In this work, we utilize the NBRA adaptation of the FSSH approach. According to it: (a) nuclei are governed by the ground state forces, regardless of electronic state transitions; (b) the nuclear velocities are not changed (rescaled or reverted) as a result of successful or frustrated hops; (c) the detailed balance is approximated by the replacing the velocity rescaling reversal by the hop acceptance criterion: the proposed hops are accepted with probability:

$$P^{\text{acc}}_{i\to j}(t,t+\Delta t) = \min\left(1, \exp\left(-\frac{E_j(t+\Delta t) - E_i(t+\Delta t)}{k_B T}\right)\right). \quad (9b)$$

In the GFSH algorithm of Wang *et al* [92, 181], all states are classified into two groups. The populations of states in group A decrease, that is $\Delta\rho_{ii} = \rho_{ii}(t+\Delta t) - \rho_{ii}(t) < 0$, $i \in A$, while the populations of states in the group B increase, $\Delta\rho_{jj} = \rho_{jj}(t+\Delta t) - \rho_{jj}(t) > 0$, $j \in B$. The hop proposal probabilities are then computed as:

$$P^{\text{prop,GFSH}}_{i\to j} = \frac{\Delta\rho_{ii}}{\rho_{ii}} \frac{\Delta\rho_{jj}}{\sum_{k\in A}\Delta\rho_{kk}}, i \in A, j \in B. \quad (10)$$

In addition to the FSSH and GFSH algorithms, we consider several decoherence correction approaches. The most straightforward modification of the FSSH algorithm is the mSDM [168] originated from the simplified decay of mixing (SDM) of Granucci *et al* [169] In these methods, the SE amplitudes, $\{c_i\}$ are modified at every time step as:

$$c_j^{'} = c_j \exp\left(-\frac{\Delta t}{\tau_{ij}}\right), \forall j \neq i \quad (11a)$$

$$c_i^{'} = c_i \sqrt{\frac{1 - \Sigma_{j\neq i}\left|c_j^{'}\right|^2}{|c_i|^2}}. \quad (11b)$$

Here index i corresponds to the currently active state and the τ_{ij} parameter corresponds to pure dephasing time for the pair of states i and j. In the original SDM formulation, the dephasing times are computed as $\tau_{I,J} = \frac{\hbar}{|E_i - E_j|}\left(1 + \frac{0.1Ha}{E_{\text{kin}}}\right)$, where $\{E_i\}$ refer to the energies of adiabatic states and E_{kin} to the nuclear kinetic energy of the system. The modification of the SDM algorithm (hence mSDM) computes the decoherence time $\tau_{i,j}$ based on the average energy gap fluctuations, δE_{ij}, following the formula of Akimov and Prezhdo [182]:

$$\tau_{i,j}{}^{-1} = \sqrt{\frac{5\langle \delta E_{ij}^2 \rangle}{12\hbar^2}}. \tag{12}$$

Another simple decoherence correction is the instantaneous decoherence (ID) approach. Following numerous prior studies [174, 183], we adopt the ID at the attempted hops (ID-A) of the Tretiak group [167], In this method, the coherent superposition is collapsed to the current active state i at every event when the hop is proposed, no matter whether the hop is accepted or not:

$$c_i = 1,\ c_j = 0,\ \forall j \neq i. \tag{13}$$

In this work, we also propose a new ID variant—the ID-F. The method is similar to the ID-A, but the state collapses, equation (13), occur at every frustrated hop instead of every attempted one. The rationale behind this approach is the following. The frustrated hops occur when the proposed hop can not accommodate the total energy balance. At such moments, no coherent superpositions can exist (since they would violate energy conservation). Thus, the wave function should be collapsed to the currently active states. The ID-F requires stronger conditions than ID-A for the collapses to occur. In fact, the hops should first be attempted. Then, the attempted hops should be rejected with the probability of $1 - \min\left(1, \exp\left(-\frac{E_j - E_i}{k_B T}\right)\right)$ probability to be considered rejected. Only under such conditions, the superposition equation (6) is collapsed according to equation (13). Finally, we also consider the DISH method of Prezhdo [170]. Unlike in FSSH and similar procedures, the hops between adiabatic states originate in this method as a result of decoherence. The initial version of DISH implemented in Libra [40] in 2021 was incorporated via the following steps.

The decoherence events are monitored. The time at which an arbitrary state i experiences a decoherence event is exponentially distributed with the corresponding decoherence time τ_i such that:

$$\frac{1}{\tau_i} = \sum_{j \neq i} r_{ij}\rho_{jj}. \tag{14}$$

Here, r_{ij} is a pure dephasing time for the pair i and j.

(a) At the decoherence event, the coherent superposition, equation (6), is collapsed onto the decohered state i with the probability $|c_i|^2$ or the decohering state is projected out of the coherent superposition with the probability $1 - |c_i|^2$;

(b) In the original prescription of Jaeger *et al* [170], one can encounter a situation in which a currently active state would experience the decoherence event and could be projected out. In this case, one runs into a problem of inconsistency between the surface hopping populations and the quantum populations, ρ_{ii}. In the revision presented earlier [40], this situation was handled as follows: if the decohered state turned out to be the active one, the corresponding amplitudes were projected out only if a successful hop to any other state could occur. In this situation, a hop to any other state j is proposed with the probability $|c_j|^2$ and if the hop into this state is successful, the superposition is collapsed onto this new state and the hop occurs.

(c) Alternatively, if the state j that experiences a decoherence event is not active, the standard procedure is applied and the hop into this state is proposed with the quantum probability $|c_j|^2$. If the hop can be accepted, the wavefunction collapses onto this state, together with the surface hop (redefining the active state).

In this work, we introduce yet another revision of the DISH algorithm, dubbed DISH_rev2023 to distinguish it from the original DISH algorithm of Jaeger *et al* as well as from the previous revision. Upon a closer examination, we realize that the prior revision of DISH may still have an intrinsic problem. In the limit of infinite decoherence times, no decoherence events would be determined and hence no hops would ever occur. In this situation, the SE populations may evolve due to NA couplings, but the TSH populations will not change, breaking the internal consistency of the method. The new approach combines elements of SDM and prior DISH as well as the FSSH hopping procedure. The central idea is to incorporate the gradual wavefunction projection process, as the original DISH procedure prescribed. Namely, the superposition equation (6) is affected by the projection operator at the decoherence events (determined in the same way as in the DISH). At these events, a state i that is considered 'decoherent' has only two outcomes: to be selected/measured by the environment with the probability of $|c_i|^2$, in which case, the superposition equation (6) is collapsed onto that state or projected out from the superposition, in which case c_i is set to zero and the rest of the superposition equation (6) is renormalized. This process somewhat resembles the gradual modification of the wavefunction amplitudes done in SDM, equetion (11), but conducted differently. Although the collapse of the superposition on the 'decoherent' pure state can be regarded as the signal for state hop to occur, in the present formulation, we consider the current DISH_rev2023 modification a decoherence correction to the SE amplitudes only (in a way the SDM or mSDM corrections work) and leaving the state hopping to be handled by the FSSH procedures. The latter accounts for both hop proposal and acceptance probabilities. The current DISH_rev2023 approach can also be thought of as a simple realization of the stochastic Schrodinger equation with a very simple dissipation-fluctuation (noise) term realized via the stochastic projection/collapse process described above.

3. Computational details

The sDFT calculations are conducted using the eQE software [128, 184] built upon QE version 5.1.0 (PWSCF code) [185]. The eQE package is used to conduct structural optimization and adiabatic molecular dynamics simulations of $2 \times 1 \times 1$ (2 pentacene molecules), $2 \times 2 \times 1$ (8 molecules), and $3 \times 3 \times 1$ supercells (18 molecules). Each supercell is broken into the indicated number of sub-systems, with a single pentacene molecule per sub-system (figure 1). The automated fragmentation Python code is used to conduct this partitioning [186].

The electronic exchange and correlation of valence electrons is described by the Perdew–Burke–Ernzerhof functional [187]. The effect of the core electrons is accounted for by the ultra-soft Vanderbilt-type pseudopotentials [188]. The valence electrons are described using the PWs basis with the wave function and charge density cutoffs of 40 Ry and 400 Ry, respectively. The dft-d2 [189] dispersion correction is also applied to improve the quality of non-bonded interactions. All calculations are conducted using the single k-point (gamma point) sampling of the Brillouin zone, which a adequate for molecular systems (individual fragments). The adiabatic molecular dynamics is conducted in the NVT ensemble with the target temperature of 300 K and nuclear integration time-step of 1 fs. The constant temperature was maintained by a velocity-rescaling thermostat [190].

In the context of sDFT, KS orbital energies of the full system are not accessible. Instead, only the orbital energies of the subsystems are available. In practice, this requires the modeler to determine ahead of time which subsystems will be 'active' and which will be 'spectators.' Such a distinction is common in fragment-based approaches, where once the fragmentation is achieved, the attention turns to only one or a few key fragments and the rest only play the role of a chemically inactive environment. Accounting for environmental effects, however, is extremely important as the environment polarizes to any chemical change in the system of interest. Thus, the environment can perturb the chemical processes making them depart from the same processes occurring in the gas phase [191–193]. Such a paradigm applies here, where the spectator subsystems, while not entering the NA-MD directly, polarize the active subsystem orbitals and orbital energies and contribute to the underlying Born–Oppenheimer dynamics on an equal footing to the active subsystem.

To conduct NA-MD calculations, we use a basis of Slater determinants composed of excitations among six frontier occupied and six unoccupied orbitals of a selected active fragment (figure 2). The present formulation is limited to the intrafragmental electronic transitions. No transitions between states of distinct fragments are allowed yet. However, the orbitals of each sub-system are determined in a self-consistent way, since orbitals of all subsystems define the embedding potential external to each of them taken individually. Thus, although there is no direct coupling of states belonging to different subsystems, there is still an indirect influence of the surrounding fragments on the states of the fragment of interest,

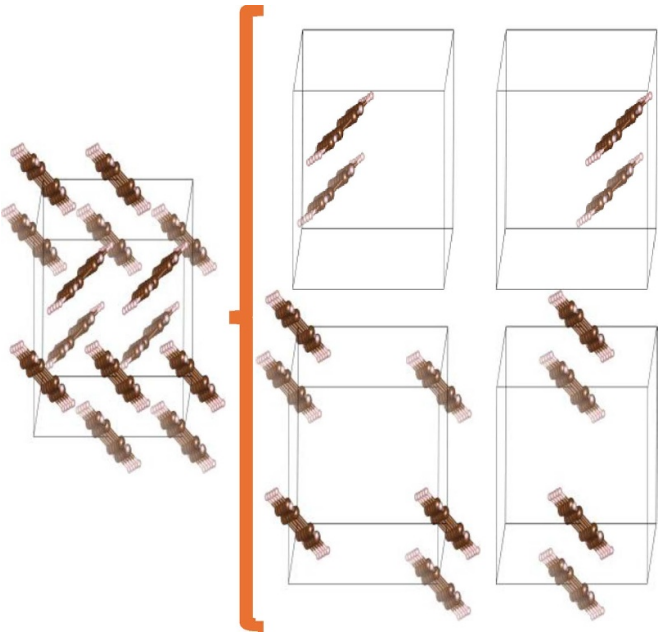

Figure 1. Schematic illustration of the partitioning of $2 \times 1 \times 1$ supercell (4 molecules) into four fragments (1 pentacene molecule per fragment), the fragments may span several periodic replicas of the original cell. The fragment sub-cells are of the same size as the original cell, corresponding to an FDE value of 1.0. In practice, smaller FDE values can be used.

which we refer to as a mutual polarization effect. The energies of such functions, $E_i(t)$, are approximated based on the sums of the KS energies, $\varepsilon_i(t)$, occupied in such determinants, $E_i(t) = \sum_{a\in i} n_a \varepsilon_a(t)$, following the earlier approach to model NA dynamics in such system [90]. Based on our calculations, excitation energy is computed as the function of time:

$$E(t) = \frac{1}{N}\sum_{i=1}^{N} p_i^{\mathrm{SH}}(t)\, E_i(t), \tag{15}$$

where N−is the total number of trajectories, $p_i^{\mathrm{SH}}(t) = \frac{N_i(t)}{N}$–is the SH population of a given state i, $N_i(t)$–is the number of trajectories associated at the time t with the adiabatic state i. The production MD trajectory runs 1.7 ps. In this study, we use $N = 250$ trajectories. The excitation energy relaxation curves are fitted to the stretched-compressed exponential fitting function, which has been used in prior studies of energy relaxation dynamics [174, 183]:

$$E(t) = E_0 \exp\left(-\left(\frac{t}{\tau}\right)^{\beta}\right), \tag{16}$$

where E_0 is initial excitation energy, chosen in this work as 2.9 eV. This value corresponds to the initial excitation to the third band of excited states (figures 5(d)–(f), vide infra). Considering the lowest excited state in our calculations is roughly at 1.0, the chosen initial electronic state corresponds to the value of excess excitation energy of 1.9 eV, which is

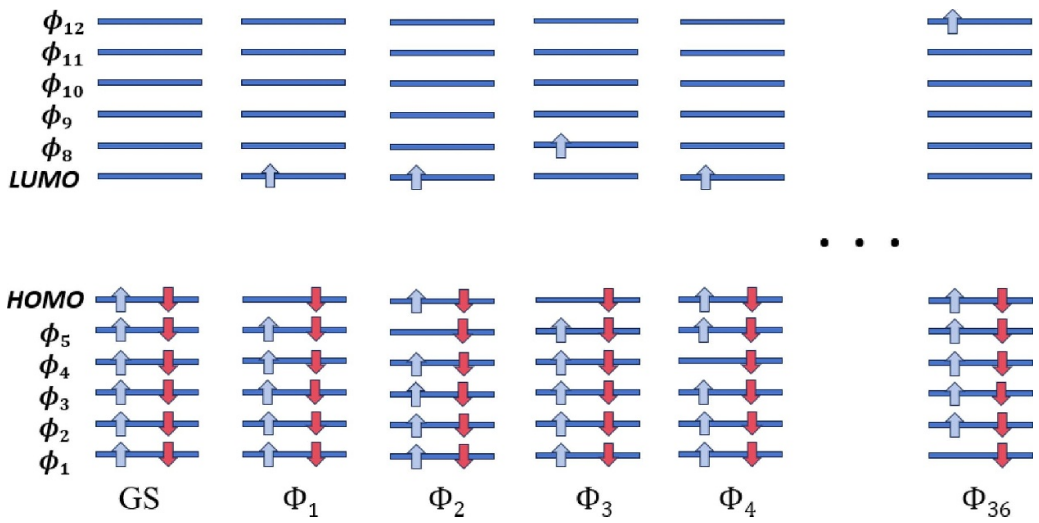

Figure 2. Single-particle excited states basis. ϕ and Φ stand for KS orbitals and Slater determines, respectively.

similar to the 1.5 eV value used in another KS-based simulation of N-MD in pentacene solids [91], β is a parameter obtained through fitting that characterizes the kinetics of the transition ($\beta \in [0, 4]$) and τ is a fitting parameter to describe the relaxation time. Fits with an R^2 factor greater than 0.8 are employed to calculate the average timescales and corresponding uncertainties/error bars within a 95% confidence interval. Each exponential fit is derived from 6 batches of surface hopping trajectories, and the final fit is averaged to yield β values shown in figure 6. The detailed scripts and codes to conduct the simulations and data analysis are available in the Zenodo repository [194].

4. Results and discussion

First, we study the convergence of static calculations on the frozen density embedding (FDE) cell split parameter (i.e. the keyword of eQE, `fde_cell_split`), see figure 3. We consider pentacene supercells of increasing size: $2 \times 1 \times 1$ (144 atoms, figure 3(a)), $2 \times 2 \times 1$ (288 atoms, figure 3(b)), and $3 \times 3 \times 1$ system (648 atoms, figure 3(c)). These systems are cut into 4, 8, and 18 fragments respectively. In each calculation, an effective fragment (subsystem) is composed of a single pentacene molecule. Every pentacene fragment resides in its own simulation cell as described in [91, 157]. The FDE parameter determines the size of a subsystem simulation cell in comparison to the size of the full (physical) cell. Thus, the FDE parameter is usually smaller than 1 for each cell lattice vector direction. The FDE parameter of 1 in all directions corresponds to using the same number of plane waves for each sub-system as the original system would use the size of the plane wave basis, it is desirable to reduce such subcells. We stress that the use of the FDE parameter does not introduce any new approximation in the physics considered by the model. It merely realizes the goal of avoiding to compute zeros. Should the simulation cell be larger than the one using the optimal FDE parameter (which is as we said less than 1) would not change the results at all and simply add space further away from the subsystem where the subsystem electron density is negligibly small. Coulomb interactions (long ranged) are always computed on the large, physical cell and thus are completely and correctly accounted for. A recent development [158] considers automatic generation of subsystem simulation cells and automatic merging/splitting of subsystems in relation to the strength of the inter-subsystem interactions. For pentacene, however, the intersubsystem interactions are always weak and therefore the subsystem definition and the simulation cells are kept unaltered throughout the simulations.

We find that the FDE values of 0.8 (figure 3(d)), 0.5 (figure 3(e)), and 0.33 (figure 3(f)) along the x direction for the $2 \times 1 \times 1$ supercell or along the (x, y) directions for both $2 \times 2 \times 1$ and $3 \times 3 \times 1$ supercells respectively, are suitable to achieve a reasonable convergence of the total energies and HOMO-LUMO gaps, yet they provide some efficiency gains. As the supercell size increases, one can choose smaller FDE values, leading to more substantial gains in the overall efficiency. The considered FDE parameters effectively reduce the number of plane waves used in the diagonalization of the KS Hamiltonian of each subsystem by 20%, 70% and 90% for $2 \times 1 \times 1$, $2 \times 2 \times 1$ and $3 \times 3 \times 1$, respectively. However, as the FDE decreases beyond the found thresholds, the effective size of the sub-cells becomes smaller than the molecular fragments leading to larger errors due to fragmentation.

The molecular dynamics simulation conducted with the chosen FDE parameters shows an increased flexibility and mobility of the pentacene molecules in the larger supercell (figure 4, panels (a)–(c)), although no critical crystal structure breaking is found at least on the timescale of this simulation. The analysis of the radial distribution functions (RDFs) of all systems (figure 4, panels (d)–(f)) suggests that structural disordering increases in the larger system—the probability distribution of having longer internuclear distances increases as one moves from the smaller supercell to the larger ones. One

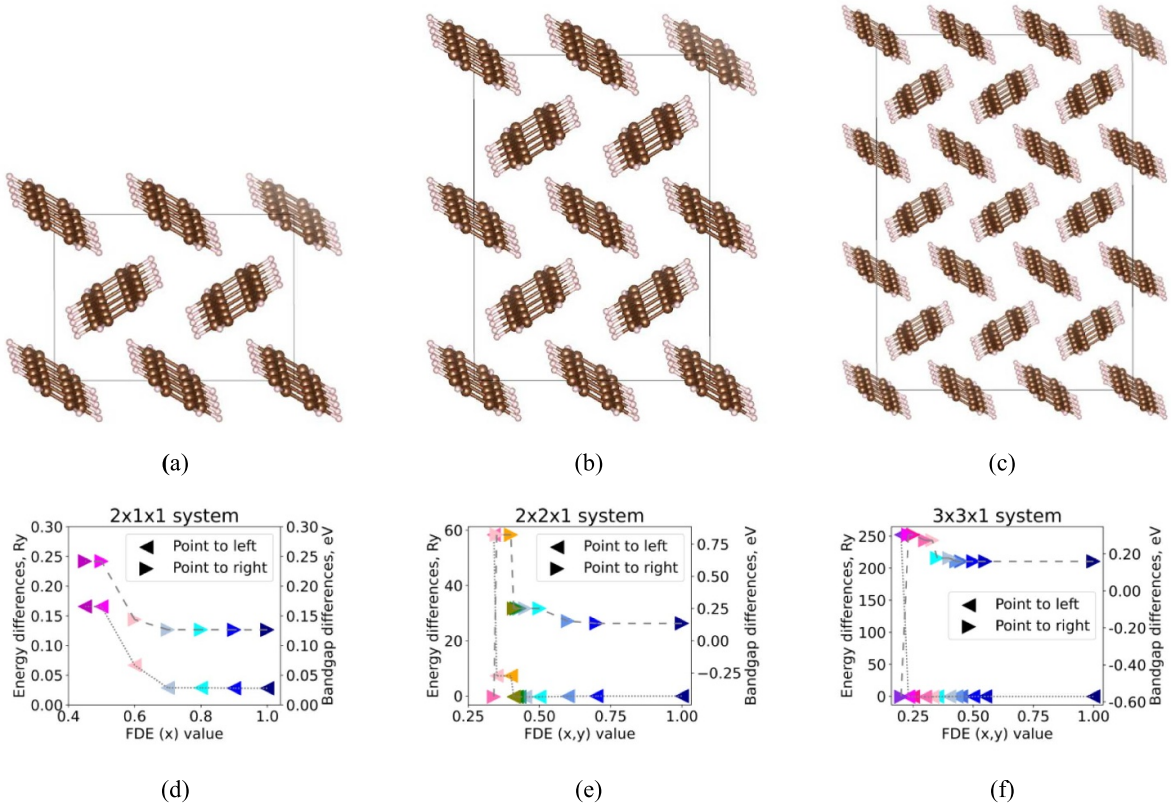

Figure 3. FDE convergence study of three supercells of pentacene crystal: (a) $2 \times 1 \times 1$ supercell (144 atoms, 4 fragments); (b) $2 \times 2 \times 1$ supercell (288 atoms, 7 or 8 fragments); (c) $3 \times 3 \times 1$ supercell (648, 18 fragments); (d)–(f) Comparison of the toal energy or HOMO-LUMO gap differences between two kinds of calculations: $\Delta X = X_{\text{QE,full system}} - X_{\text{eQE,subsystems}}$ the convergence for X being the total energy (left-arrow triangles) and HOMO-LUMO gap (right-arrow triangles). The FDE values in cyan are the ones chosen for the calculations in the non-adiabatic dynamic: (d) FDE = 0.8; (e) FDE = 0.5; (f) FDE = 0.33. Supercells are constructed and visualized using VESTA [195] software.

can also observe the RDF values for the distances between 4 and 5 Angstrom decrease when moving from the $2 \times 1 \times 1$ to the $2 \times 2 \times 1$ system. We attribute this change to the relaxing of the artificial correlation of the pentacene molecules' motion present in the smallest supercell. Doubling the size of the supercell enables more flexibility in the relative orientation of each of the two pairs of pentacene molecules with respect to each other. Going further, to the $3 \times 3 \times 1$ supercell, the RDF values in the 4–5 Angstrom range do not change significantly. However, the slope of the longer-distance tail of the RDF distribution decreases, suggesting the increase of the long-range disorder in the larger supercell, consistent with the visualization of molecular motion (e.g. figure 4(c)).

In general, the increased size of the supercell promotes stronger disorder. This can be understood by the fact that such a system has an increased number of independent molecules that can evolve in an increasingly uncorrelated way compared to their motion in smaller supercells. The dynamics of the crystals with only 2 pentacene molecules per supercell is much more affected by spurious correlations since the closest periodic images the two pentacene molecules of the central cell move in the same way as such molecules themselves. The disordering of pentacene molecules is facilitated by the weaker intermolecular and dispersion interactions in this system and the high range of temperature fluctuations in our NVT simulations with temperature in the 300 ± 100 K interval. Although with such fluctuations, the instantaneous temperature of the system is well below the pentacene's normal melting point, the lack of dispersion correction in the present functional lowers the computational melting temperature. Thus, the disordering is observed in the present study already at the 300 ± 100 K interval. The disordering is artificially prevented in smaller supercells due to the artificial correlation of motion of pentacene molecules

To characterize the effect of polarization of pentacene fragments by other pentacene molecules present in the crystal, we compute the total densities of states and evolutions of KS orbital energies (figures 5(a)–(c)), the evolution of the excitation energies of a selected fragment (figure 5, panels (d)–(f)), and the average magnitudes of absolute NACs between excited Slater determinants of this fragment considered in this work (figure 5, panels (g)–(i)). The comparison across different sizes of supercells (columns in figure 5) shows no notable differences in densities of states or state energies. The only major difference is in the NAC maps—the frequency of larger NAC values is increasing in the larger systems

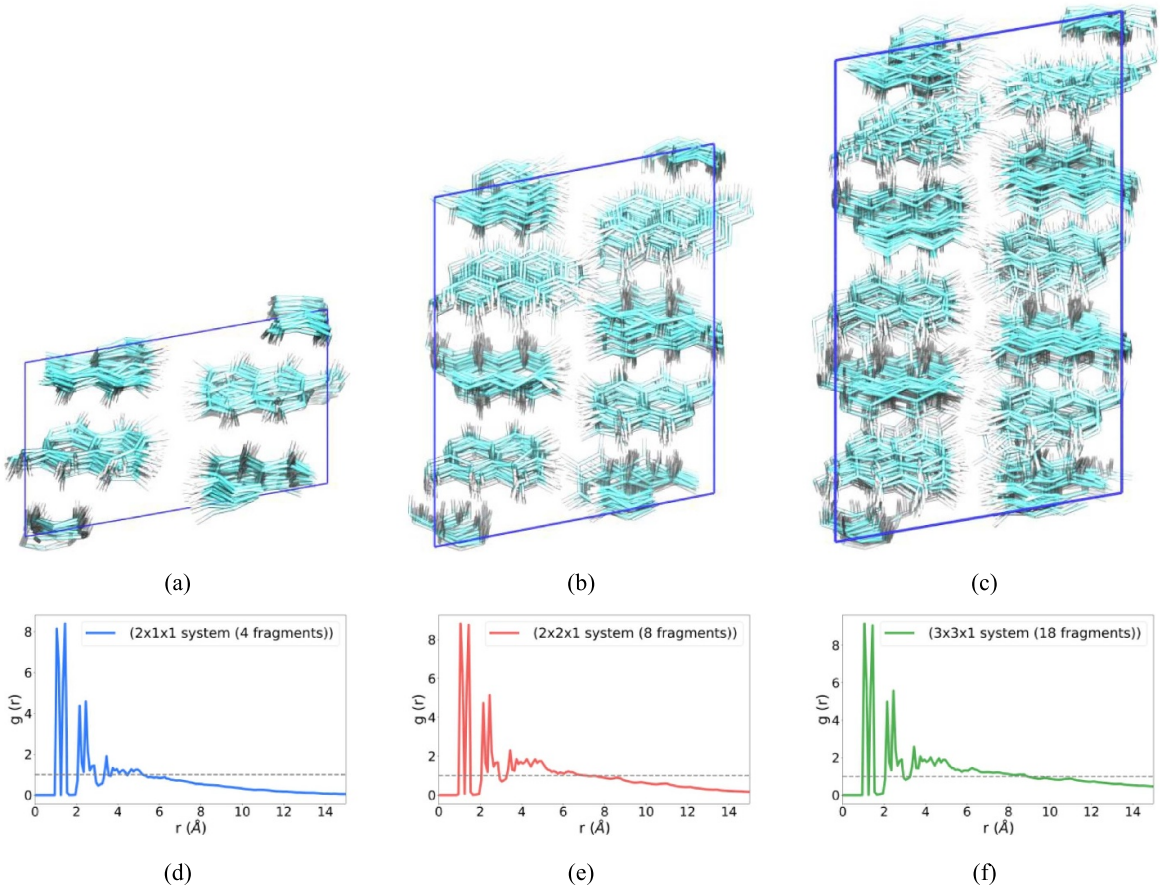

Figure 4. Characterization of nuclear structure and dynamics of pentacene systems by the visual molecular dynamics (VMD) [196]: (a), (d) $2 \times 1 \times 1$ supercell; (b), (e) $2 \times 2 \times 1$ supercell; (c), (f) $3 \times 3 \times 1$ supercell. The first row (a)–(c) shows the configurations sampled by the MD trajectories: it suggests greater mobility and configurational freedom of pentacene molecules in larger supercells; (d)–(f) radial distribution functions for three supercells—shows an increased long-range disorder in larger systems.

(figure 5(i)). We attribute this effect to the larger conformational flexibility of pentacene in larger supercells. The NAC quantifies the coupling of electronic and nuclear degrees of freedom. Thus, the more pronounced intermolecular vibrations as well as slight angular motion of pentacene in large systems induce more notable changes of pentacene orbitals and hence lead to larger NACs. We emphasize here that although we consider the NACs for the orbitals belonging to the same pentacene fragment, these NACs are enhanced by the inter- rather than intra-molecular interactions. Indeed, in a more disordered $3 \times 3 \times 1$ supercell, orbitals of the same molecule may be affected to different extents by the polarization and exchange effects due to the environment of other fragments. Thus, the motion of the environmental fragments on the supercell size as well as on the choice of the NA-MD can induce stronger dissimilarities in the evolution of different orbitals of the same fragment, leading to increased NACs.

Next, we explore the dependence of NA-MD dynamics on the methodology (figure 6). Namely, we analyze the excitation energy decay times obtained from the fits of the averaged excitation energy decay curves to the stretched-compressed exponential decay law, equation (16). There are two main observations. First, the energy relaxation accelerates in the larger ($3 \times 3 \times 1$) system, whereas there are no significant differences in relaxation times for the smaller ($2 \times 1 \times 1$ and $2 \times 2 \times 1$) supercells. This effect can be rationalized by the disorder effects and the correspondingly increased NACs in the larger system. We should note that in the present work, the increased disordering is caused by the lack of proper interactions that would stabilize the crystal at this simulation temperature. In this regard, one should be careful relating the computed timescales to relevant experimental data on pentacene crystals. However, this effect is still physical and is interesting from the perspective of the system near its phase transition point. Having dispersion corrections would simply result in such an effect occurring at higher temperatures. Thus, a convergence is indeed observed in the sequence of $2 \times 1 \times 1$ and $2 \times 2 \times 1$ systems. The significant deviation of the timescales computed for $3 \times 3 \times 1$ supercell is attributed to the finite-size effects enhance dynamical disorder of the nuclear system due to weak dispersion correction in the present version of eQE. The possibility of such structural and dynamical reorganization is enabled by an increased independence of motion of fragments in the larger supercell.

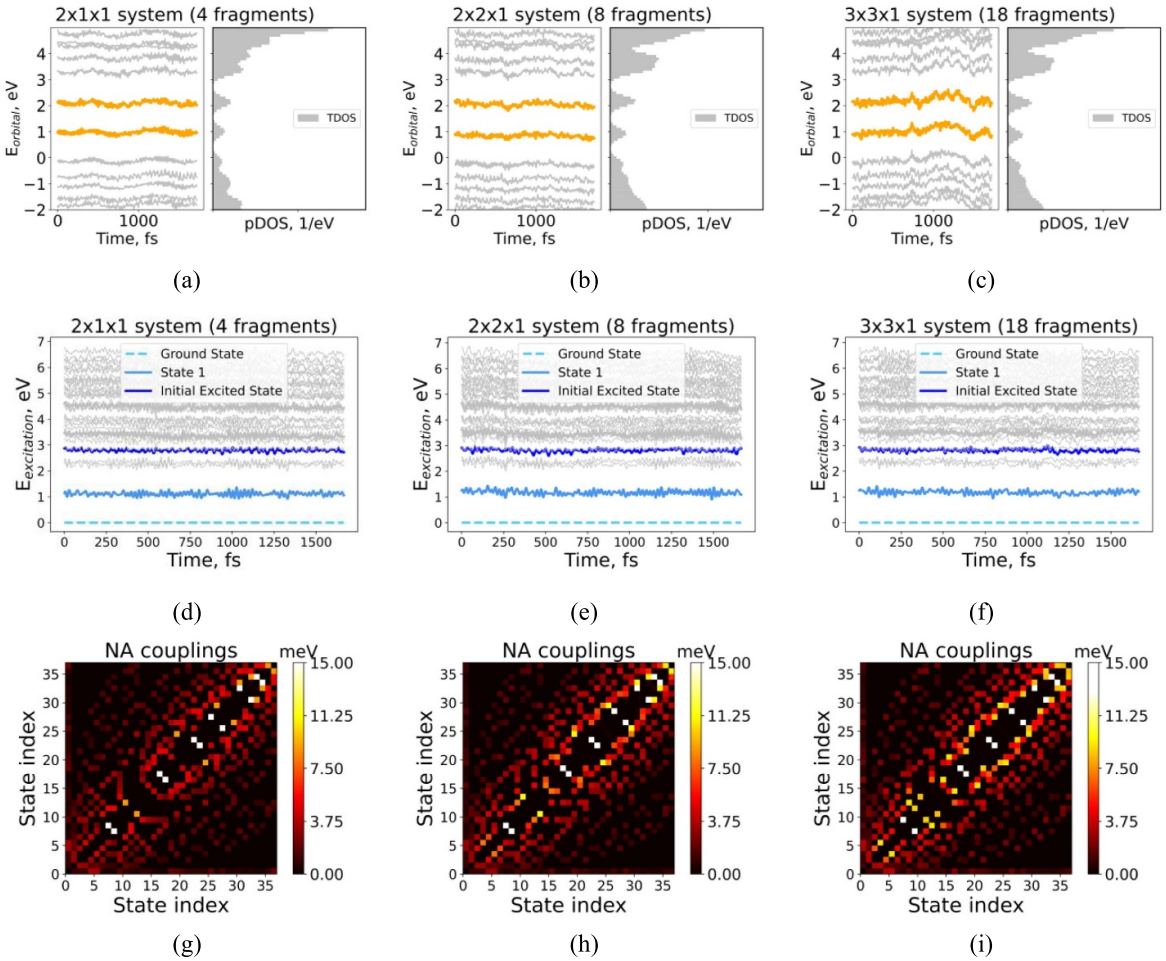

Figure 5. Characterization of electronic structure properties of pentacene supercells. (a)–(c) partial densities of states of pentacene fragments in different environments; (d)–(f) evolution of state energies for states of the pentacene systems in different environments; (g)–(i) average magnitudes of nonadiabatic couplings connecting all pairs of 36 states considered in this work. Columns correspond to different supercell sizes: (a), (d), (g) $2 \times 1 \times 1$ system; (b), (e), (h) $2 \times 2 \times 1$ system; (c), (f), (i) $3 \times 3 \times 1$ system.

The second observation concerns the relative magnitudes of the excitation energy relaxation timescales. The computed dynamics falls within one of the two groups of methods. The first group includes the FSSH, GFSH, DISH, IDA, and IDF. All these methods predict relatively fast energy relaxation with the timescales ranging from 1.2 to 2.3 ps for $2 \times 1 \times 1$ and $2 \times 2 \times 1$ supercells or from 0.7 to 1.3 ps for the $3 \times 3 \times 1$ supercell depending on the method. For each given method, the timescales in the $3 \times 3 \times 1$ supercell are about twice as small as the corresponding values in the $2 \times 1 \times 1$ or $2 \times 2 \times 1$ supercells. The excitation energy decays to a value close to zero, suggest- ing that the relaxation to the ground state is also very fast (on this timescale), which is likely a significant overestimation, considering such processes often occur on the order of hundreds of picoseconds—dozens of nanoseconds. Although methods like DISH, IDA, and IDF are considered the methods that incorporate decoherence corrections, they are likely insufficient for this kind of problem. In fact, the new variation of the DISH method yields the timescales comparable to those of the overcoherent FSSH and GFSH methods. In this regard, the new variation of DISH does not lead to deceleration of the excitation energy relaxation expected in simulations with decoherence-corrected methods [174, 183, 197]. The dynamics generated by the IDF method is similar to that of the IDA, which suggest that there is no much difference in whether the wave function collaps occurs at attempted or at frustrated hops, at least for this kind of systems. The second group of methods includes only the mSDM method. Unlike all other approaches, this method suggests 13–14 ps relaxation times for $2 \times 1 \times 1$ and $2 \times 2 \times 1$ systems and about 8 ps for the $3 \times 3 \times 1$ system. In addition, the excitation energy does not decay to zero value, suggesting that this timescale corresponds to relaxation dynamics of higher excited states relaxing to the lowest excitation. No recovery of the ground state occurs, in better agreement with empirical knowledge. Thus, the decoherence correction introduced by the mSDM seems to be more reliable for the present problem.

Finally, we comment on the obtained timescales. First, the 0.7–2.0 ps timescales obtained with methods other than mSDM may nominally be related to the 600–700 fs hot carrier

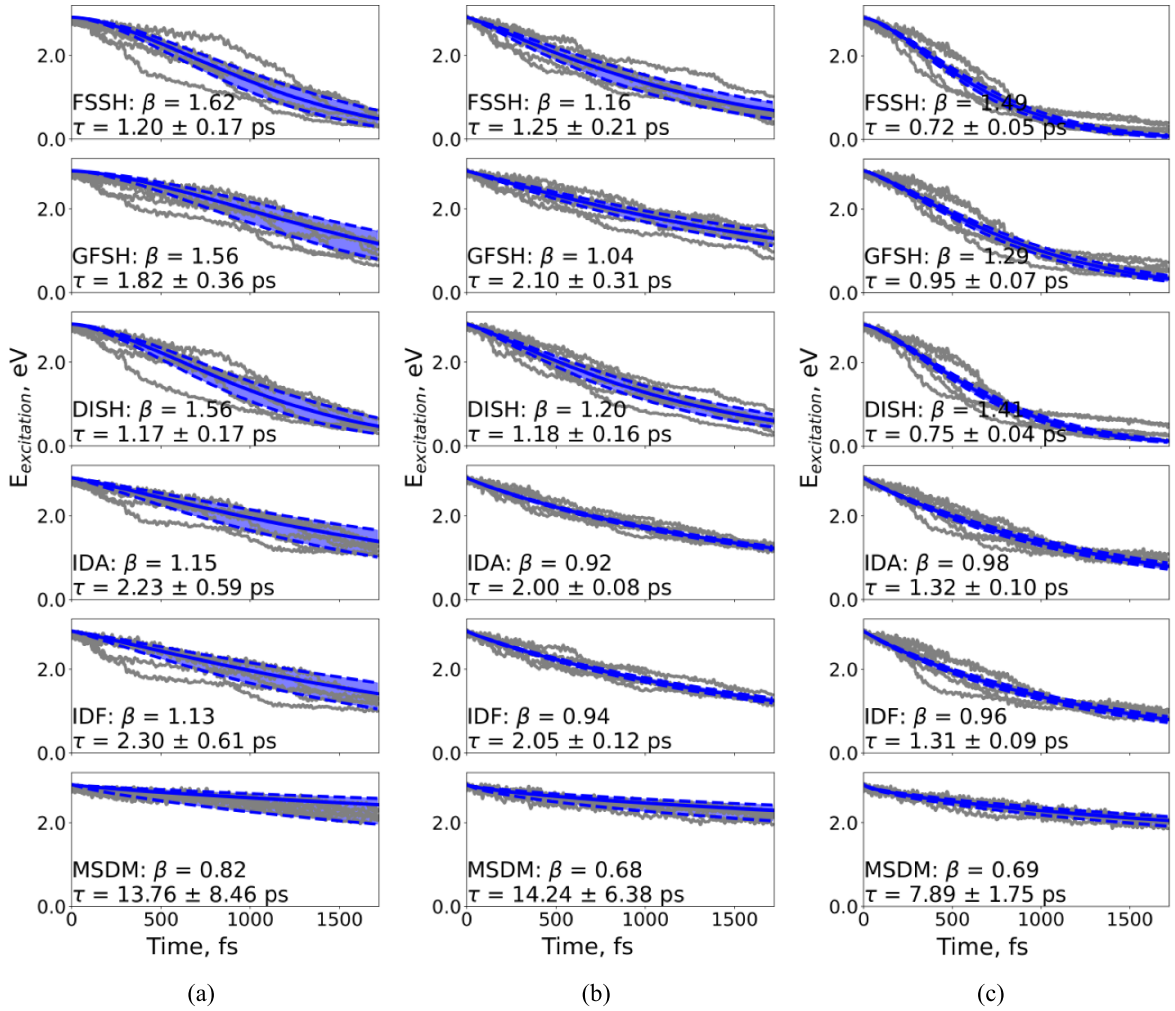

Figure 6. Excitation energy relaxation dynamics for three supercell sizes: (a) $2 \times 1 \times 1$; (b) $2 \times 2 \times 1$; and (c) $3 \times 3 \times 1$. The calculations are conducted with different methods. From top down: FSSH, GFSH, DISH, IDA, IDF, and mSDM. Grey lines represent the dynamics for different batches, while blue lines represent the fits of the average excitation energy excess over all batches ($R^2 > 0.8$) together with the corresponding confidence intervals.

relaxation timescales reported experimentally [198, 199] for solid pentacene. However, one should keep in mind that solid pentacene has an increased density of electronic states that may not be directly related to the density of single-fragment states even though they are obtained keeping all other fragments in mind. Thus, one may expect that the timescales obtained for such an isolated fragment may be overestimated compared to the experimental counterparts. In this regard, only the timescales obtained with the mSDM may be more reasonable. Acceleration of the dynamics by the increased density of states would make the timescales obtained with other methods in a poorer comparison to the experimental values, while the current mSDM timescales of 8–14 ps may come to a closer agreement with the experiment. In addition, the current approach is based on a simplistic description of electronic excited states as excited Slater determinants whose energies are evaluated based on orbital energy differences. A more realistic description of excited states of pentacene via TD-DFT would likely result in stronger coupling of such many-body states (mixing different excited Slater determinants) and would further accelerate the dynamics, as was already demonstrated in prior studies on other systems. Finally, the fact that the present guiding trajectories are based on the adiabatic dynamics guided by the ground state PES means that nuclear geometries sampled by such dynamics may be more distant from the configurations with stronger NACs. This would result in an additional overestimation of relaxation timescales. Evolving nuclear trajectories on excited PESs is likely to result in geometries that are closer to strong NAC regions and hence are more likely to result in faster relaxation. Thus, yet again the apparent 8–14 ps timescales obtained with mSDM may be a reasonable upper limit of the true timescales for hot excited state relaxation. The values in the 0.7–2 ps range obtained with other methods may become much smaller after including effects due to many-body nature of excited states, higher density of states of crystalline pentacene, and potential non-NBRA corrections of nuclear trajectories.

5. Conclusions

In this paper, we present a sDFT/NA-MD methodology for modeling NA processes in large periodic systems that can be partitioned into weakly interacting molecular fragments. The developed approach is implemented via an interface of the open-source eQE and Libra software packages. We find that while the initial increase of the minimal supercell of pentacene from the $2 \times 1 \times 1$ to the $2 \times 2 \times 1$ does not change the timescales of the nonadiabatic relaxation of excitation energy, increasing the supercell further to $3 \times 3 \times 1$ size accelerates this process due to increased degree of dynamical and structural disorder in such a system. The increased disorder facilitates the change of the Gaussian relaxation kinetics in favor of the exponential one. We find a strong dependence of the relaxation timescales on the methodology used—for most methods, the timescales vary in the range of 0.7–2.0 ps. They are smaller for methods lacking decoherence corrections such as FSSH and GFSH and for the larger $3 \times 3 \times 1$ supercell. Out of all tested methods, only mSDM is capable of yielding significantly slower relaxation times ranging from 13–14 ps in smaller systems to about 8 ps in the more disordered $3 \times 3 \times 1$ supercell. However, we argue that such value is a reasonable upper estimate to true excitation energy excess relaxation timescales, which may better agree with the experiment after accounting for many-body effects, higher density of states in periodic pentacene, and non-NBRA dynamics of nuclear trajectories. Finally, we find that the new modification of the DISH (DISH_rev2023) and the new variation of the ID method (ID-F) do not show significant improvement in regard of their ability to capture electronic decoherence effects and perform similar to FSSH/GFSH and ID-A, respectively.

Data availability statement

The data that support the findings of this study are openly available at the following URL/DOI: https://doi.org/10.5281/zenodo.11018262.

Acknowledgments

A V A acknowledges the financial support of the National Science Foundation (Grant NSF-2045204). Support of computations was provided by the Center for Computational Research at the University at Buffalo. W M acknowledges funding support from the National Natural Science Foundation of China under Grant No. 12274171. W L acknowledges the financial support from the National Natural Science Foundation of China (No. 22373033). M P acknowledges funding from the National Science Foundation under Grant Nos. CHE-2154760, OAC-2321103 and a Grant by DOE BES CTC program.

ORCID iDs

Michele Pavanello https://orcid.org/0000-0001-8294-7481
Alexey V Akimov https://orcid.org/0000-0002-7815-3731

References

[1] Nelson N and Ben-Shem A 2004 The complex architecture of oxygenic photosynthesis *Nat. Rev. Mol. Cell Biol.* **5** 971–82
[2] Hedges M P, Longdell J J, Li Y and Sellars M J 2010 Efficient quantum memory for light *Nature* **465** 1052–6
[3] Mittal S, Goldschmidt E A and Hafezi M 2018 A topological source of quantum light *Nature* **561** 502–6
[4] Rodt S, Reitzenstein S and Heindel T 2020 Deterministically fabricated solid-state quantum-light sources *J. Phys.: Condens. Matter* **32** 153003
[5] Romero E, Novoderezhkin V I and Van Grondelle R 2017 Quantum design of photosynthesis for bio-inspired solar-energy conversion *Nature* **543** 355–65
[6] Cao J *et al* 2020 Quantum biology revisited *Sci. Adv.* **6** eaaz4888
[7] Dohnalová K, Gregorkiewicz T and Kůsová K 2014 Silicon quantum dots: surface matters *J. Phys.: Condens. Matter* **26** 173201
[8] Piccardo M *et al* 2022 Roadmap on multimode light shaping *J. Opt.* **24** 013001
[9] Krause K D, Rees K and Algar W R 2023 Assessing the steric impact of surface ligands on the proteolytic turnover of quantum dot–peptide conjugates *ACS Appl. Mater. Interfaces* **15** 57799–811
[10] Li Y *et al* 2023 Azobenzene as a photoswitchable mechanophore *Nat. Chem.* **16** 446–55
[11] Gieseking R L, Ratner M A and Schatz G C 2016 Review of plasmon-induced hot-electron dynamics and related SERS chemical effects *ACS Symposium Series* vol 1245, ed Y Ozaki, G C Schatz, D Graham and T Itoh (American Chemical Society) pp 1–22
[12] Takata T, Jiang J, Sakata Y, Nakabayashi M, Shibata N, Nandal V, Seki K, Hisatomi T and Domen K 2020 Photocatalytic water splitting with a quantum efficiency of almost unity *Nature* **581** 411–4
[13] Yuan Y, Jin N, Saghy P, Dube L, Zhu H and Chen O 2021 Quantum Dot Photocatalysts for Organic Transformations *J. Phys. Chem. Lett.* **12** 7180–93
[14] Zhang Y, Li Y, Xin X, Wang Y, Guo P, Wang R, Wang B, Huang W, Sobrido A J and Li X 2023 Internal quantum efficiency higher than 100% achieved by combining doping and quantum effects for photocatalytic overall water splitting *Nat. Energy* **8** 504–14
[15] Rao C N R, Cheetham A K and Thirumurugan A 2008 Hybrid inorganic–organic materials: a new family in condensed matter physics *J. Phys.: Condens. Matter* **20** 083202
[16] Hazarika A, Zhao Q, Gaulding E A, Christians J A, Dou B, Marshall A R, Moot T, Berry J J, Johnson J C and Luther J M 2018 Perovskite quantum dot photovoltaic materials beyond the reach of thin films: full-range tuning of a-site cation composition *ACS Nano* **12** 10327–37
[17] Giannini S and Blumberger J 2022 Charge transport in organic semiconductors: the perspective from nonadiabatic molecular dynamics *Acc. Chem. Res.* **55** 819–30

[18] Li D, Jia M, Jia T and Chen G 2024 Ultrasensitive NIR-II ratiometric nanothermometers for 3D in vivo thermal imaging *Adv. Mater.* **36** 2309452

[19] Nwaji N, Gwak J, Nguyen M-C, Nguyen H-Q, Kang H, Choi Y, Kim Y, Chen H and Lee J 2024 Emerging potentials of Fe-based nanomaterials for chiral sensing and imaging *Med. Res. Rev.* **44** 897–918

[20] Orihashi K, Yamauchi A, Fujiwara S, Asada M, Nakamura T, Ka-Ho Hui J, Kimizuka N, Tateishi K, Uesaka T and Yanai N 2023 Spin-polarized radicals with extremely long spin–lattice relaxation time at room temperature in a metal–organic framework *J. Am. Chem. Soc.* **145** 27650–6

[21] Tyryshkin A M, Morton J J L, Benjamin S C, Ardavan A, Briggs G A D, Ager J W and Lyon S A 2006 Coherence of spin qubits in silicon *J. Phys.: Condens. Matter* **18** S783–94

[22] Matsuo S *et al* 2023 Phase-dependent Andreev molecules and superconducting gap closing in coherently-coupled Josephson junctions *Nat. Commun.* **14** 8271

[23] Meyer M, Déprez C, Meijer I N, Unseld F K, Karwal S, Sammak A, Scappucci G, Vandersypen L M K and Veldhorst M 2023 Single-electron occupation in quantum dot arrays at selectable plunger gate voltage *Nano Lett.* **23** 11593–600

[24] Irgen-Gioro S, Gururangan K, Saer R G, Blankenship R E and Harel E 2019 Electronic coherence lifetimes of the Fenna–Matthews–Olson complex and light harvesting complex II *Chem. Sci.* **10** 10503–9

[25] Hu Z, Liu Z and Sun X 2022 Effects of heterogeneous protein environment on excitation energy transfer dynamics in the Fenna–Matthews–Olson complex *J. Phys. Chem.* B **126** 9271–87

[26] Dani R, Kundu S and Makri N 2023 Coherence maps and flow of excitation energy in the bacterial light harvesting complex 2 *J. Phys. Chem. Lett.* **14** 3835–43

[27] Yoneda Y *et al* 2021 Electron–nuclear dynamics accompanying proton-coupled electron transfer *J. Am. Chem. Soc.* **143** 3104–12

[28] Zhang J, Borrelli R and Tanimura Y 2021 Probing photoinduced proton coupled electron transfer process by means of two-dimensional resonant electronic–vibrational spectroscopy *J. Chem. Phys.* **154** 144104

[29] Warburton R E, Soudackov A V and Hammes-Schiffer S 2022 Theoretical modeling of electrochemical proton-coupled electron transfer *Chem. Rev.* **122** 10599–650

[30] Shukla K, Chen P-S, Chen J-R, Chang Y-H and Liu Y-W 2020 Macroscopic matter wave quantum tunneling *Commun. Phys.* **3** 101

[31] Yang P-Y and Cao J 2021 Quantum effects in chemical reactions under polaritonic vibrational strong coupling *J. Phys. Chem. Lett.* **12** 9531–8

[32] Yu X, Zhang X and Wang J 2023 Fully electrically controlled van der Waals multiferroic tunnel junctions *ACS Nano* **17** 25348–56

[33] Scholes G D *et al* 2017 Using coherence to enhance function in chemical and biophysical systems *Nature* **543** 647–56

[34] Barbatti M, Aquino A J A, Szymczak J J, Nachtigallová D, Hobza P and Lischka H 2010 Relaxation mechanisms of UV-photoexcited DNA and RNA nucleobases *Proc. Natl Acad. Sci. USA* **107** 21453–8

[35] Giussani A and Worth G A 2020 On the intrinsically low quantum yields of pyrimidine DNA photodamages: evaluating the reactivity of the corresponding minimum energy crossing points *J. Phys. Chem. Lett.* **11** 4984–9

[36] Casacio C A, Madsen L S, Terrasson A, Waleed M, Barnscheidt K, Hage B, Taylor M A and Bowen W P 2021 Quantum-enhanced nonlinear microscopy *Nature* **594** 201–6

[37] Toldo J M, Do Casal M T and Barbatti M 2021 Mechanistic aspects of the photophysics of UVA filters based on meldrum derivatives *J. Phys. Chem.* A **125** 5499–508

[38] Abiola T T *et al* 2021 New generation UV-A filters: understanding their photodynamics on a human skin mimic *J. Phys. Chem. Lett.* **12** 337–44

[39] Akimov A V and Prezhdo O V 2014 Advanced capabilities of the PYXAID program: integration schemes, decoherence effects, multiexcitonic states, and field-matter interaction *J. Chem. Theory Comput.* **10** 789–804

[40] Akimov A V 2021 Excited state dynamics in monolayer black phosphorus revisited: accounting for many-body effects *J. Chem. Phys.* **155** 134106

[41] Zimmerman P M, Zhang Z and Musgrave C B 2010 Singlet fission in pentacene through multi-exciton quantum states *Nat. Chem.* **2** 648–52

[42] Berkelbach T C, Hybertsen M S and Reichman D R 2013 Microscopic theory of singlet exciton fission. I. General formulation *J. Chem. Phys.* **138** 114102

[43] Congreve D N, Lee J, Thompson N J, Hontz E, Yost S R, Reusswig P D, Bahlke M E, Reineke S, Van Voorhis T and Baldo M A 2013 External quantum efficiency above 100% in a singlet-exciton-fission–based organic photovoltaic cell *Science* **340** 334–7

[44] Berkelbach T C, Hybertsen M S and Reichman D R 2014 Microscopic theory of singlet exciton fission. III. Crystalline pentacene *J. Chem. Phys.* **141** 074705

[45] Akimov A V and Prezhdo O V 2014 Nonadiabatic dynamics of charge transfer and singlet fission at the pentacene/C_{60} interface *J. Am. Chem. Soc.* **136** 1599–608

[46] Broch K *et al* 2018 Robust singlet fission in pentacene thin films with tuned charge transfer interactions *Nat. Commun.* **9** 954

[47] C A Valente D, Do Casal M T, Barbatti M, Niehaus T A, Aquino A J A, Lischka H and Cardozo T M 2021 Excitonic and charge transfer interactions in tetracene stacked and T-shaped dimers *J. Chem. Phys.* **154** 044306

[48] Dimitrov S D and Durrant J R 2014 Materials design considerations for charge generation in organic solar cells *Chem. Mater.* **26** 616–30

[49] Zhang L, Shu Y, Sun S and Truhlar D G 2021 Direct coherent switching with decay of mixing for intersystem crossing dynamics of thioformaldehyde: the effect of decoherence *J. Chem. Phys.* **154** 094310

[50] Wang X, Wu C, Wang Z and Liu W 2023 When do tripdoublet states fluoresce? A theoretical study of copper(II) porphyrin *Front. Chem.* **11** 1259016

[51] Akimov A V, Muckerman J T and Prezhdo O V 2013 Nonadiabatic dynamics of positive charge during photocatalytic water splitting on GaN(10–10) surface: charge localization governs splitting efficiency *J. Am. Chem. Soc.* **135** 8682–91

[52] Wang L, Akimov A and Prezhdo O V 2016 Recent progress in surface hopping: 2011–2015 *J. Phys. Chem. Lett.* **7** 2100–12

[53] Oberhofer H, Reuter K and Blumberger J 2017 Charge transport in molecular materials: an assessment of computational methods *Chem. Rev.* **117** 10319–57

[54] Li W, She Y, Vasenko A S and Prezhdo O V 2021 *Ab initio* nonadiabatic molecular dynamics of charge carriers in metal halide perovskites *Nanoscale* **13** 10239–65

[55] Hruska E, Husek J, Bandaranayake S and Baker L R 2022 Visible light absorption and hot carrier trapping in anatase TiO_2: the role of surface oxygen vacancies *J. Phys. Chem.* C **126** 10752–61

[56] da Silva M A R *et al* Single-atoms on crystalline carbon nitrides for selective C-H photooxidation: a bridge to achieve homogeneous pathways in heterogeneous materials *Adv. Mater.* **35** 2304152

[57] Li H *et al* 2024 Structure and defect engineering synergistically boost high solar-to-chemical conversion efficiency of cerium oxide/Au hollow nanomushrooms for nitrogen photofixation *Angew. Chem., Int. Ed* **63** e202316384

[58] Liu Z, Xie Y, Liu L, Cai X, Yin H-Q, Zuo M, Liu Y, Feng S, Huang W and Wu D π-sticked metal−organic monolayers for single-metal-site dependent CO_2 photoreduction and hydrogen evolution reaction *Small* **20** 2309194

[59] Wu X *et al* 2023 Bioinspired polyoxo-titanium cluster for greatly enhanced solar-driven CO_2 reduction *Nano Lett.* **23** 11562–8

[60] Babapoor-Farrokhran S *et al* 2023 Pathologic vs. protective roles of hypoxia-inducible factor 1 in RPE and photoreceptors in wet vs. dry age-related macular degeneration *Proc. Natl Acad. Sci. USA* **120** e2302845120

[61] Hahn J *et al* 2023 Evolution of neuronal cell classes and types in the vertebrate retina *Nature* **624** 415–24

[62] Jiang B *et al* 2023 Light-induced LLPS of the CRY2/SPA1/FIO1 complex regulating mRNA methylation and chlorophyll homeostasis in Arabidopsis *Nat. Plants* **9** 2042–58

[63] Käb G 2004 Statistical mechanics of mean field ehrenfest quantum/classical molecular dynamics: the damped harmonic oscillator *J. Phys. Chem.* A **108** 8866–77

[64] Subotnik J E 2010 Augmented Ehrenfest dynamics yields a rate for surface hopping *J. Chem. Phys.* **132** 134112

[65] Tully J C 1990 Molecular dynamics with electronic transitions *J. Chem. Phys.* **93** 1061–71

[66] Tully J C 1998 Mixed quantum–classical dynamics *Faraday Discuss.* **110** 407–19

[67] Hack M D and Truhlar D G 2000 Nonadiabatic trajectories at an exhibition *J. Phys. Chem.* A **104** 7917–26

[68] Donoso A and Martens C C 2001 Quantum tunneling using entangled classical trajectories *Phys. Rev. Lett.* **87** 223202

[69] Webster F, Wang E T, Rossky P J and Friesner R A 1994 Stationary phase surface hopping for nonadiabatic dynamics: two-state systems *J. Chem. Phys.* **100** 4835–47

[70] Prezhdo O V 2021 Modeling non-adiabatic dynamics in nanoscale and condensed matter systems *Acc. Chem. Res.* **54** 4239–49

[71] Smith B and Akimov A V 2020 Modeling nonadiabatic dynamics in condensed matter materials: some recent advances and applications *J. Phys.: Condens. Matter* **32** 073001

[72] Li X *et al* 2022 Ultrafast spontaneous localization of a Jahn-teller exciton polaron in two-dimensional semiconducting CrI_3 by symmetry breaking *Nano Lett.* **22** 8755–62

[73] Yin Y, Zhao X, Ren X, Liu K, Zhao J, Zhang L and Li S 2022 Thickness dependent ultrafast charge transfer in BP/MoS_2 heterostructure *Adv. Funct. Mater.* **32** 2206952

[74] Zhou Z, He J, Frauenheim T, Prezhdo O V and Wang J 2022 Control of hot carrier cooling in lead halide perovskites by point defects *J. Am. Chem. Soc.* **144** 18126–34

[75] Wang S, Huang M, Wu Y-N, Chu W, Zhao J, Walsh A, Gong X-G, Wei S-H and Chen S 2022 Effective lifetime of non-equilibrium carriers in semiconductors from non-adiabatic molecular dynamics simulations *Nat. Comput. Sci.* **2** 486–93

[76] Wang X, Gao W and Zhao J 2022 Strain modulation of the exciton anisotropy and carrier lifetime in black phosphorene *Phys. Chem. Chem. Phys.* **24** 10860–8

[77] Liu J, Zhang X and Lu G 2022 Non-adiabatic exciton dynamics in van der Waals heterostructures *J. Phys. Chem. Lett.* **13** 11760–9

[78] Liu H *et al* 2023 Atomic-scale manipulation of single-polaron in a two-dimensional semiconductor *Nat. Commun.* **14** 3690

[79] Zheng Z, Shi Y, Zhou J-J, Prezhdo O V, Zheng Q and Zhao J 2023 Ab initio real-time quantum dynamics of charge carriers in momentum space *Nat. Comput. Sci.* **3** 532–41

[80] Waters M D J, Casanova J T and Wörner H J 2023 Ultrafast dissociation of nitromethane from the 3p Rydberg state *Mol. Phys.* **121** e2164749

[81] Puentes-Milián L, García-Alfonso E, Márquez-Mijares M and Rubayo-Soneira J 2023 NeI $_2$ photofragmentation dynamics through quasiclassical and semiclassical studies *ChemPhysChem* **24** e202300406

[82] Agrawal S, Lin W, Prezhdo O V and Trivedi D J 2020 *Ab initio* quantum dynamics of charge carriers in graphitic carbon nitride nanosheets *J. Chem. Phys.* **153** 054701

[83] Borges I, Guimarães R M P O, Monteiro-de-castro G, Rosa N M P, Nieman R, Lischka H and Aquino A J A 2023 A comprehensive analysis of charge transfer effects on donor-pyrene (bridge)-acceptor systems using different substituents *J. Comput. Chem.* **44** 2424–36

[84] Guo H, Zhang X and Lu G 2023 Pseudo-heterostructure and condensation of 1D moiré excitons in twisted phosphorene bilayers *Sci. Adv.* **9** eadi5404

[85] Silva A J F W H D S, Rodrigues G P, Ventura E and Do Monte S A 2024 Photodissociation and formation of an ion-pair in CH_2FCL (HCFC -31) *J. Comput. Chem.* **45** 476–86

[86] Nelson T R, White A J, Bjorgaard J A, Sifain A E, Zhang Y, Nebgen B, Fernandez-Alberti S, Mozyrsky D, Roitberg A E and Tretiak S 2020 Non-adiabatic excited-state molecular dynamics: theory and applications for modeling photophysics in extended molecular materials *Chem. Rev.* **120** 2215–87

[87] Madjet M E-A, Ali E, Carignano M, Vendrell O and Chakraborty H S 2021 Ultrafast transfer and transient entrapment of photoexcited Mg electron in Mg @ C 60 *Phys. Rev. Lett.* **126** 183002

[88] Tinnin J, Bhandari S, Zhang P, Geva E, Dunietz B D, Sun X and Cheung M S 2022 Correlating interfacial charge transfer rates with interfacial molecular structure in the tetraphenyldibenzoperiflanthene/C_{70} organic photovoltaic system *J. Phys. Chem. Lett.* **13** 763–9

[89] Hu Z and Sun X 2022 All-atom nonadiabatic semiclassical mapping dynamics for photoinduced charge transfer of organic photovoltaic molecules in explicit solvents *J. Chem. Theory Comput.* **18** 5819–36

[90] Craig C F, Duncan W R and Prezhdo O V 2005 Trajectory surface hopping in the time-dependent kohn-sham approach for electron-nuclear dynamics *Phys. Rev. Lett.* **95** 163001

[91] Akimov A V and Prezhdo O V 2013 The PYXAID program for non-adiabatic molecular dynamics in condensed matter systems *J. Chem. Theory Comput.* **9** 4959–72

[92] Wang L, Trivedi D and Prezhdo O V 2014 Global flux surface hopping approach for mixed quantum-classical dynamics *J. Chem. Theory Comput.* **10** 3598–605

[93] Araujo L, Lasser C and Schmidt B 2024 FSSH-2: fewest switches surface hopping with robust switching probability *J. Chem. Theory Comput.* **20** 3413–9

[94] Granucci G, Persico M and Toniolo A 2001 Direct semiclassical simulation of photochemical processes with semiempirical wave functions *J. Chem. Phys.* **114** 10608–15

[95] Meek G A and Levine B G 2014 Evaluation of the time-derivative coupling for accurate electronic state transition probabilities from numerical simulations *J. Phys. Chem. Lett.* **5** 2351–6

[96] Shakiba M and Akimov A V 2023 Generalization of the local diabatization approach for propagating electronic degrees of freedom in nonadiabatic dynamics *Theor. Chem. Acc.* **142** 68

[97] Fernandez-Alberti S, Roitberg A E, Nelson T and Tretiak S 2012 Identification of unavoided crossings in nonadiabatic photoexcited dynamics involving multiple electronic states in polyatomic conjugated molecules *J. Chem. Phys.* **137** 014512

[98] Wang L and Prezhdo O V 2014 A simple solution to the trivial crossing problem in surface hopping *J. Phys. Chem. Lett.* **5** 713–9

[99] Wang Z, Dong J and Wang L 2023 Large-scale surface hopping simulation of charge transport in hexagonal molecular crystals: role of electronic coupling signs *J. Phys.: Condens. Matter* **35** 345401

[100] Akimov A V 2016 Nonadiabatic molecular dynamics with tight-binding fragment molecular orbitals *J. Chem. Theory Comput.* **12** 5719–36

[101] Akimov A V and Prezhdo O V 2015 Analysis of self-consistent extended Hückel theory (SC-EHT): a new look at the old method *J. Math. Chem.* **53** 528–50

[102] Rego L G C and Batista V S 2003 Quantum dynamics simulations of interfacial electron transfer in sensitized TiO $_2$ semiconductors *J. Am. Chem. Soc.* **125** 7989–97

[103] Rego L G C, Rocha A R, Rodrigues V and Ugarte D 2003 Role of structural evolution in the quantum conductance behavior of gold nanowires during stretching *Phys. Rev.* B **67** 045412

[104] Gieseking R L M 2019 Third-order nonlinear optical properties of Ag nanoclusters: connecting molecule-like and nanoparticle-like behavior *Chem. Mater.* **31** 6850–9

[105] Fabiano E, Keal T W and Thiel W 2008 Implementation of surface hopping molecular dynamics using semiempirical methods *Chem. Phys.* **349** 334–47

[106] Dewar M J S and Thiel W 1977 Ground states of molecules. 38. The MNDO method. Approximations and parameters *J. Am. Chem. Soc.* **99** 4899–907

[107] Tretiak S, Saxena A, Martin R L and Bishop A R 2000 CEO/semiempirical calculations of UV–visible spectra in conjugated molecules *Chem. Phys. Lett.* **331** 561–8

[108] Nelson T, Fernandez-Alberti S, Roitberg A E and Tretiak S 2014 Nonadiabatic excited-state molecular dynamics: modeling photophysics in organic conjugated materials *Acc. Chem. Res.* **47** 1155–64

[109] Tretiak S, Chernyak V and Mukamel S 1996 Collective electronic oscillators for nonlinear optical response of conjugated molecules *Chem. Phys. Lett.* **259** 55–61

[110] Song H, Nam Y, Keefer D, Garavelli M, Mukamel S and Tretiak S 2021 Nonadiabatic molecular dynamics study of the relaxation pathways of photoexcited cyclooctatetraene *J. Phys. Chem. Lett.* **12** 5716–22

[111] da Silva Oliboni R, Bortolini G, Torres A and Rego L G C 2016 A nonadiabatic excited state molecular mechanics/extended hückel ehrenfest method *J. Phys. Chem.* C **120** 27688–98

[112] Akimov A V 2016 Libra: an open-Source "methodology discovery" library for quantum and classical dynamics simulations: SOFTWARE NEWS AND UPDATES *J. Comput. Chem.* **37** 1626–49

[113] Pal S, Trivedi D J, Akimov A V, Aradi B, Frauenheim T and Prezhdo O V 2016 Nonadiabatic molecular dynamics for thousand atom systems: a tight-binding approach toward PYXAID *J. Chem. Theory Comput.* **12** 1436–48

[114] Stojanović L, Aziz S G, Hilal R H, Plasser F, Niehaus T A and Barbatti M 2017 Nonadiabatic dynamics of cycloparaphenylenes with TD-DFTB surface hopping *J. Chem. Theory Comput.* **13** 5846–60

[115] Cui Q, Elstner M, Kaxiras E, Frauenheim T and Karplus M 2001 A QM/MM implementation of the self-consistent charge density functional tight binding (SCC-DFTB) method *J. Phys. Chem.* B **105** 569–85

[116] Liu Y, Zheng F, Dai H, Chen C, Chen Y, Wu H, Yu C, Mai Y, Frauenheim T and Zhou Y 2023 Insight into the molecular mechanism for enhanced longevity of supramolecular vesicular photocatalysts *Angew. Chem., Int. Ed* **62** e202302126

[117] Shakiba M, Stippell E, Li W and Akimov A V 2022 Nonadiabatic molecular dynamics with extended density functional tight-binding: application to nanocrystals and periodic solids *J. Chem. Theory Comput.* **18** 5157–80

[118] Shakiba M and Akimov A V 2023 Dependence of electron–hole recombination rates on charge carrier concentration: a case study of nonadiabatic molecular dynamics in graphitic carbon nitride monolayers *J. Phys. Chem.* C **127** 9083–96

[119] Stanton R and Trivedi D J 2023 Charge carrier dynamics at the interface of 2D metal–organic frameworks and hybrid perovskites for solar energy harvesting *Nano Lett.* **23** 11932–9

[120] Dral P O, Barbatti M and Thiel W 2018 Nonadiabatic excited-state dynamics with machine learning *J. Phys. Chem. Lett.* **9** 5660–3

[121] Zhou G, Chu W and Prezhdo O V 2020 Structural deformation controls charge losses in $MAPbI_3$: unsupervised machine learning of nonadiabatic molecular dynamics *ACS Energy Lett.* **5** 1930–8

[122] Akimov A V 2021 Extending the time scales of nonadiabatic molecular dynamics via machine learning in the time domain *J. Phys. Chem. Lett.* **12** 12119–28

[123] Shao X, Paetow L, Tuckerman M E and Pavanello M 2023 Machine learning electronic structure methods based on the one-electron reduced density matrix *Nat. Commun.* **14** 6281

[124] Shakiba M and Akimov A V 2024 Machine-learned Kohn–Sham hamiltonian mapping for nonadiabatic molecular dynamics *J. Chem. Theory Comput.* **20** 2992–3007

[125] Uratani H and Nakai H 2020 Non-adiabatic molecular dynamics with divide-and-conquer type large-scale excited-state calculations *J. Chem. Phys.* **152** 224109

[126] Wang L-W, Lee B, Shan H, Zhao Z, Meza J, Strohmaier E and Bailey D H 2008 Linearly scaling 3D fragment method for large-scale electronic structure calculations *2008 SC—Int. Conf. for High Performance Computing, Networking, Storage and Analysis* (*Austin, TX, USA*) (IEEE) pp 1–10

[127] Wang Z, Dong J, Qiu J and Wang L 2022 All-atm nonadiabatic dynamics simulation of hybrid graphene nanoribbons based on wannier analysis and machoine learning *ACS Appl. Mater. Interfaces* **14** 22929–40

[128] Genova A, Ceresoli D, Krishtal A, Andreussi O, DiStasio R A Jr and Pavanello M 2017 eQE: an open-source density functional embedding theory code for the condensed phase *Int. J. Quantum Chem.* **117** e25401

[129] Jacob C R and Neugebauer J 2014 Subsystem density-functional theory *Wiley Interdiscip. Rev. Comput. Mol. Sci.* **4** 325–62

[130] Krishtal A, Sinha D, Genova A and Pavanello M 2015 Subsystem density-functional theory as an effective tool for modeling ground and excited states, their dynamics, and many-body interactions *J. Phys.: Condens. Matter* **27** 183202

[131] Wesolowski T A, Shedge S and Zhou X 2015 Frozen-density embedding strategy for multilevel simulations of electronic structure *Chem. Rev.* **115** 5891–928

[132] Jacob C R and Neugebauer J 2024 Subsystem density-functional theory (update) *Wiley Interdiscip. Rev. Comput. Mol. Sci.* **14** e1700

[133] Genova A, Ceresoli D and Pavanello M 2016 Avoiding fractional electrons in subsystem DFT based *ab-initio* molecular dynamics yields accurate models for liquid water and solvated OH radical *J. Chem. Phys.* **144** 234105
[134] Mi W, Ramos P, Maranhao J and Pavanello M 2019 Ab initio structure and dynamics of CO_2 at supercritical conditions *J. Phys. Chem. Lett.* **10** 7554–9
[135] Bensberg M, Türtscher P L, Unsleber J P, Reiher M and Neugebauer J 2022 Solvation free energies in subsystem density functional theory *J. Chem. Theory Comput.* **18** 723–40
[136] Chakravarty C, Aksu H, Martinez B J A, Ramos P, Pavanello M and Dunietz B D 2022 Role of dielectric screening in calculating excited states of solvated azobenzene: a benchmark study comparing quantum embedding and polarizable continuum model for representing the solvent *J. Phys. Chem. Lett.* **13** 4849–55
[137] Massolle A and Neugebauer J 2020 Subsystem density-functional theory for interacting open-shell systems: spin densities and magnetic exchange couplings *Faraday Discuss.* **224** 201–26
[138] Andermatt S, Cha J, Schiffmann F and VandeVondele J 2016 Combining linear-scaling DFT with subsystem DFT in born–oppenheimer and ehrenfest molecular dynamics simulations: from molecules to a virus in solution *J. Chem. Theory Comput.* **12** 3214–27
[139] Scholz L and Neugebauer J 2021 Protein response effects on cofactor excitation energies from first principles: augmenting subsystem time-dependent density-functional theory with many-body expansion techniques *J. Chem. Theory Comput.* **17** 6105–21
[140] Niemeyer N *et al* 2023 The subsystem quantum chemistry program serenity *WIREs Comput. Mol. Sci.* **13** e1647
[141] Neugebauer J 2010 Chromophore-specific theoretical spectroscopy: from subsystem density functional theory to mode-specific vibrational spectroscopy *Phys. Rep.* **489** 1–87
[142] Shao X, Umerbekova A, Jiang K and Pavanello M 2022 Many-body van der waals interactions in wet MoS_2 surfaces *Electron. Struct.* **4** 024001
[143] König C and Neugebauer J 2013 Protein Effects on the optical spectrum of the Fenna–Matthews–Olson complex from fully quantum chemical calculations *J. Chem. Theory Comput.* **9** 1808–20
[144] Unsleber J P, Dresselhaus T, Klahr K, Schnieders D, Böckers M, Barton D and Neugebauer J 2018 Serenity: a subsystem quantum chemistry program *J. Comput. Chem.* **39** 788–98
[145] Mališ M and Luber S 2021 ΔSCF with subsystem density embedding for efficient nonadiabatic molecular dynamics in condensed-phase systems *J. Chem. Theory Comput.* **17** 1653–61
[146] Vandaele E, Mališ M and Luber S 2022 The ΔSCF method for non-adiabatic dynamics of systems in the liquid phase *J. Chem. Phys.* **156** 130901
[147] Shakiba M, Smith B, Li W, Dutra M, Jain A, Sun X, Garashchuk S and Akimov A 2022 Libra: a modular software library for quantum nonadiabatic dynamics *Softw. Impacts* **14** 100445
[148] Alam B, Morrison A F and Herbert J M 2020 Charge separation and charge transfer in the low-lying excited states of pentacene *J. Phys. Chem.* C **124** 24653–66
[149] Bhattacharyya A, Sahu A, Patra S and Tiwari V 2023 Low and high frequency vibrations synergistically enhance singlet exciton fission through robust vibronic resonances *Proc. Natl Acad. Sci. USA* **120** e2310124120
[150] Hou Y, Papadopoulos I, Bo Y, Wollny A-S, Ferguson M J, Mai L A, Tykwinski R R and Guldi D M 2023 Catalyzing singlet fission by transition metals: second versus third row effects *Precis. Chem.* **1** 555–64
[151] Shu Y, Lim Y-F, Li Z, Purushothaman B, Hallani R, Kim J E, Parkin S R, Malliaras G G and Anthony J E 2011 A survey of electron-deficient pentacenes as acceptors in polymer bulk heterojunction solar cells *Chem. Sci.* **2** 363–8
[152] El Jouad Z, El-Menyawy E M, Louarn G, Arzel L, Morsli M, Addou M, Bernède J C and Cattin L 2020 The effect of the band structure on the Voc value of ternary planar heterojunction organic solar cells based on pentacene, boron subphthalocyanine chloride and different electron acceptors *J. Phys. Chem. Solids* **136** 109142
[153] Çaldıran Z, Erkem Ü, Baltakesmez A and Biber M 2021 Effects of the PENTACENE as doping material on the power conversion efficiency of P3HT:PCBM based ternary organic solar cells *Physica* B **607** 412859
[154] Schön J, Kloc C, Bucher E and Batlogg B 2000 Efficient organic photovoltaic diodes based on doped pentacene *Nature* **403** 408–10
[155] Kera S *et al* 2013 Experimental reorganization energies of pentacene and perfluoropentacene: effects of perfluorination *J. Phys. Chem.* C **117** 22428–37
[156] Seiler H, Krynski M, Zahn D, Hammer S, Windsor Y W, Vasileiadis T, Pflaum J, Ernstorfer R, Rossi M and Schwoerer H 2021 Nuclear dynamics of singlet exciton fission in pentacene single crystals *Sci. Adv.* **7** eabg0869
[157] Baumgärtner K *et al* 2022 Ultrafast orbital tomography of a pentacene film using time-resolved momentum microscopy at a FEL *Nat. Commun.* **13** 2741
[158] Kim Y W, Lee D, Jeon Y, Yoo H, Cho E-S, Darici E, Park Y-J, Seo K-I and Kwon S-J 2023 Analyses of all small molecule-based pentacene/C60 organic photodiodes using vacuum evaporation method *Nanomaterials* **13** 2820
[159] Wang L, Olivier Y, Prezhdo O V and Beljonne D 2014 Maximizing singlet fission by intermolecular packing *J. Phys. Chem. Lett.* **5** 3345–53
[160] Zeng T, Hoffmann R and Ananth N 2014 The low-lying electronic states of pentacene and their roles in singlet fission *J. Am. Chem. Soc.* **136** 5755–64
[161] López X, Straatsma T P, Sánchez-Mansilla A and de Graaf C 2023 Non-orthogonal configuration interaction study on the effect of thermal distortions on the singlet fission process in photoexcited pure and B,N-doped pentacene crystals *J. Phys. Chem.* C **127** 16249–58
[162] Zhu X-Y, Yang Q and Muntwiler M 2009 Charge-transfer excitons at organic semiconductor surfaces and interfaces *Acc. Chem. Res.* **42** 1779–87
[163] Jacob C R, Neugebauer J and Visscher L 2008 A flexible implementation of frozen-density embedding for use in multilevel simulations *J. Comput. Chem.* **29** 1011–8
[164] Jacob C R, Beyhan S M, Bulo R E, Gomes A S P, Götz A W, Kiewisch K, Sikkema J and Visscher L 2011 PyADF—a scripting framework for multiscale quantum chemistry *J. Comput. Chem.* **32** 2328–38
[165] Höfener S, Severo Pereira Gomes A and Visscher L 2012 Molecular properties via a subsystem density functional theory formulation: a common framework for electronic embedding *J. Chem. Phys.* **136** 044104
[166] Luber S 2014 Local electric dipole moments for periodic systems via density functional theory embedding *J. Chem. Phys.* **141** 234110
[167] Nelson T, Fernandez-Alberti S, Roitberg A E and Tretiak S 2013 Nonadiabatic excited-state molecular dynamics: treatment of electronic decoherence *J. Chem. Phys.* **138** 224111
[168] Smith B and Akimov A V 2019 A comparative analysis of surface hopping acceptance and decoherence algorithms within the neglect of back-reaction approximation *J. Chem. Phys.* **151** 124107

[169] Granucci G, Persico M and Zoccante A 2010 Including quantum decoherence in surface hopping *J. Chem. Phys.* **133** 134111
[170] Jaeger H M, Fischer S and Prezhdo O V 2012 Decoherence-induced surface hopping *J. Chem. Phys.* **137** 22A545
[171] Chu W, Zheng Q, Prezhdo O V, Zhao J and Saidi W A 2020 Low-frequency lattice phonons in halide perovskites explain high defect tolerance toward electron-hole recombination *Sci. Adv.* **6** eaaw7453
[172] Plasser F, Granucci G, Pittner J, Barbatti M, Persico M and Lischka H 2012 Surface hopping dynamics using a locally diabatic formalism: charge transfer in the ethylene dimer cation and excited state dynamics in the 2-pyridone dimer *J. Chem. Phys.* **137** 22A514
[173] Löwdin P-O 1955 Quantum theory of many-particle systems. I. Physical interpretations by means of density matrices, natural spin-orbitals, and convergence problems in the method of configurational interaction *Phys. Rev.* **97** 1474–89
[174] Smith B, Shakiba M and Akimov A V 2021 Nonadiabatic dynamics in si and CdSe nanoclusters: many-body vs single-particle treatment of excited states *J. Chem. Theory Comput.* **17** 678–93
[175] Vanderbilt D 1990 Soft self-consistent pseudopotentials in a generalized eigenvalue formalism *Phys. Rev.* B **41** 7892–5
[176] Qian X, Li J, Lin X and Yip S 2006 Time-dependent density functional theory with ultrasoft pseudopotentials: real-time electron propagation across a molecular junction *Phys. Rev.* B **73** 035408
[177] Walker B and Gebauer R 2007 Ultrasoft pseudopotentials in time-dependent density-functional theory *J. Chem. Phys.* **127** 164106
[178] Deng Z-Y and Feng H-J 2022 Real-time first-principles calculations of ultrafast carrier dynamics of SnSe/TiO_2 heterojunction under Li^+ implantation *J. Phys.: Condens. Matter* **34** 355001
[179] Akimov A V 2018 A simple phase correction makes a big difference in nonadiabatic molecular dynamics *J. Phys. Chem. Lett.* **9** 6096–102
[180] Shenvi N, Subotnik J E and Yang W 2011 Phase-corrected surface hopping: correcting the phase evolution of the electronic wavefunction *J. Chem. Phys.* **135** 024101
[181] Wang L, Sifain A E and Prezhdo O V 2015 Communication: global flux surface hopping in Liouville space *J. Chem. Phys.* **143** 191102
[182] Akimov A V and Prezhdo O V 2013 Persistent electronic coherence despite rapid loss of electron–nuclear correlation *J. Phys. Chem. Lett.* **4** 3857–64
[183] Smith B, Shakiba M and Akimov A V 2021 Crystal symmetry and static electron correlation greatly accelerate nonradiative dynamics in lead halide perovskites *J. Phys. Chem. Lett.* **12** 2444–53
[184] Mi W, Shao X, Genova A, Ceresoli D and Pavanello M 2021 eQE 2.0: subsystem DFT beyond GGA functionals *Comput. Phys. Commun.* **269** 108122
[185] Giannozzi P *et al* 2009 QUANTUM ESPRESSO: a modular and open-source software project for quantum simulations of materials *J. Phys.: Condens. Matter* **21** 395502
[186] Pavanello M 2017 *eQE Gitlab* (available at: https://Gitlab.Com/Pavanello/Eqe)
[187] Perdew J P, Burke K and Ernzerhof M 1996 Generalized gradient approximation made simple *Phys. Rev. Lett.* **77** 3865–8
[188] Kresse G and Joubert D 1999 From ultrasoft pseudopotentials to the projector augmented-wave method *Phys. Rev.* B **59** 1758–75
[189] Grimme S 2004 Accurate description of van der Waals complexes by density functional theory including empirical corrections *J. Comput. Chem.* **25** 1463–73
[190] Woodcock L V 1971 Isothermal molecular dynamics calculations for liquid salts *Chem. Phys. Lett.* **10** 257–61
[191] Skinner O S, Catherman A D, Early B P, Thomas P M, Compton P D and Kelleher N L 2014 Fragmentation of integral membrane proteins in the gas phase *Anal. Chem.* **86** 4627–34
[192] Gunaratne K D D, Prabhakaran V, Johnson G E and Laskin J 2015 Gas-phase fragmentation pathways of mixed addenda keggin anions: $pMo_{12-n}W_nO_{40}^{3-}$ (n = 0–12) *J. Am. Soc. Mass Spectrom.* **26** 1027–35
[193] Gholipour-Ranjbar H, Jena P and Laskin J 2022 Gas-phase fragmentation of single heteroatom-incorporated $Co_5MS_8(PEt_3)_6^+$ (M = Mn, Fe, Co, Ni) nanoclusters *Commun. Chem.* **5** 130
[194] Zhang Q and Akimov A 2024 *AkimovLab/Project_Libra-eQE: v1.0.0 (v1.0.0)* (Zenodo) (https://doi.org/10.5281/zenodo.11018262)
[195] Momma K and Izumi F 2011 VESTA 3 for three-dimensional visualization of crystal, volumetric and morphology data *J. Appl. Crystallogr.* **44** 1272–6
[196] Humphrey W, Dalke A and Schulten K 1996 VMD: visual molecular dynamics *J. Mol. Graph.* **14** 33–38
[197] Akimov A V 2024 Fundamentals of trajectory-based methods for nonadiabatic dynamics *Comprehensive Computational Chemistry* (Elsevier) pp 235–72
[198] Thorsmølle V K, Averitt R D, Demsar J, Smith D L, Tretiak S, Martin R L, Chi X, Crone B K, Ramirez A P and Taylor A J 2009 Photoexcited carrier relaxation dynamics in pentacene probed by ultrafast optical spectroscopy: influence of morphology on relaxation processes *Physica* B **404** 3127–30
[199] Wilson M W B, Rao A, Ehrler B and Friend R H 2013 Singlet exciton fission in polycrystalline pentacene: from photophysics toward devices *Acc. Chem. Res.* **46** 1330–8